

Toward a Unified Parameterization of the Boundary Layer and Moist Convection. Part II: Lateral Mass Exchanges and Subplume-Scale Fluxes

CARA-LYN LAPPEN AND DAVID A. RANDALL

Department of Atmospheric Sciences, Colorado State University, Fort Collins, Colorado

(Manuscript received 18 July 2000, in final form 31 January 2001)

ABSTRACT

The dissipation parameterizations developed for higher-order closure are used to parameterize lateral entrainment and detrainment in a mass-flux model. In addition, a subplume-scale turbulence scheme is included to represent fluxes not captured in the conventional mass-flux framework. These new parameterizations are tested by simulating trade wind cumulus from the Barbados Oceanographic and Meteorological Experiment (BOMEX).

1. Introduction

In Part I of this paper (Lappen and Randall 2001a, hereafter LR1), we presented a framework with which we can unify mass-flux and higher-order closure (MFC and HOC, respectively) within a single system of equations. By accomplishing this, we can draw from two substantial preexisting knowledge bases to create one model—an exercise in “cross-fertilization.” This model (named Assumed-Distribution Higher-Order Closure, or ADHOC) makes use of an assumed joint probability density distribution for the variables of interest, and the equations typically used in HOC models can be derived by integrating over the distribution (Lappen 1999). We believe that this approach has the potential to represent boundary layer turbulence, shallow cumulus convection, and possibly even deep cumulus convection, all within a unified framework.

In the process of unifying these two very different systems, we encountered two immediate challenges. First, lateral mass exchanges between updrafts and downdrafts (or between updrafts and their environment) are explicitly accounted for in mass-flux models, whose equations are derived using updraft–downdraft [“tophat” probability density function (PDF)] decompositions; such exchanges are not explicitly represented in HOC models because updraft–downdraft entities are not explicitly defined in such models. In the mass-flux equations, mass exchanges are represented in terms of entrainment (E) and detrainment (D), which refer to air crossing into and out of the updraft, respectively. Since HOC models have been successfully applied to bound-

ary layers in which entrainment and detrainment are important physical processes [e.g., trade wind cumulus layers (Yamada and Mellor 1979; Bechtold et al. 1995)], entrainment and detrainment must somehow be implicitly represented in the HOC equations. We showed in LR1 that these processes work through the dissipation terms of the HOC equations [this was independently noticed by de Roode et al. (2000)]. ADHOC’s new parameterization of lateral entrainment and detrainment (discussed in section 2) is directly based on the analogy between the E and D terms in MFC and the dissipation terms in the HOC equations.

The second challenge was to include the effects of subplume-scale (SPS) turbulence in ADHOC. Interestingly enough, although SPS motions have never been explicitly represented in *either* MFC or HOC models, the importance of their effects emerges when the two theories are combined. This can be understood if we consider the typical scales that MFC and HOC models were designed to represent, and how these models were typically implemented.

- The ensemble-averaged statistics in conventional HOC models are *supposed* to represent all scales, and thus have had no need for a separate small-scale eddy parameterization.
- Most mass-flux models applied to the planetary boundary layer (PBL) have been used in conjunction with a mixed-layer model (e.g., Wang and Albrecht 1986), and thus have made use of linear flux profiles.

However, it has been found by Businger and Oncley (1990), Young (1988), Schumann and Moeng (1991), and Wyngaard and Moeng (1992) for the convective boundary layer and by Schumann and Moeng (1991), Wang and Stevens (2000), and de Laat and Duynkerke (1998) for the stratus-topped boundary layer that the

Corresponding author address: Dr. Cara-Lyn Lappen, Department of Atmospheric Science, Colorado State University, Fort Collins, CO 80523.
E-mail: lappen@atmos.colostate.edu

tophat contribution captures only about 60% of thermodynamic fluxes. In cumulus layers, the tophat contribution was found to be 80–90% for the fluxes of conserved variables (except near cloud base) and considerably less for the fluxes of nonconserved variables (Siebesma and Cuijpers 1995; Wang and Stevens 2000).

Siebesma and Cuijpers (1995, hereafter SC95) showed [using results from a large-eddy simulation (LES)] that in order to accurately represent the total flux in a mass-flux model, the SPS effects must be considered. The relevance of these studies to ADHOC (or to mass-flux models in general) is clear if one considers that a tophat PDF for a given variable consists of only two possible values: one for the updraft and one for the downdraft. Thus, a vertical flux of, say, temperature is represented in terms of the correlation of the one updraft (downdraft) value of vertical velocity with the one updraft (downdraft) value of temperature. In reality, however, a range of updraft and downdraft vertical velocities and temperatures can contribute to the flux. Since the smaller-scale fluctuations cannot be represented in the tophat framework, they can be thought of as an SPS contribution to the flux.

Petersen et al. (1999) showed that a simulation of the convective boundary layer using mass-flux schemes is significantly affected by the SPS fluxes (i.e., the part of the flux that is not resolved explicitly by the mass-flux formulas). They ran several tests with different mass-flux schemes in “stand alone” mode (they prescribed the boundary layer height, updraft area fraction, and convective mass flux; i.e., they did not actually run a mass-flux model) and compared the results to those of LES. They concluded that the best performance is obtained with mass-flux schemes that use the exact plume-budget equations (as used in ADHOC; see LR1). In addition, they showed that, in order to accurately model the lateral mass exchange terms, it is necessary to account for mass exchanges between updrafts and downdrafts (something that we also explicitly do in ADHOC; see section 2). They concluded that the SPS contributions to the fluxes must be included in order to accurately model the convective PBL with a mass-flux model.

Petersen et al. (1999) were the first (to our knowledge) to address the issue of SPS effects in a mass-flux model. The current study is the first attempt to actually implement an SPS parameterization in such a model. We can make the analogy between ADHOC and LES models: LES models resolve the large eddies and parameterize the small eddies with a subgrid-scale (SGS) scheme (Deardorff 1972; Moeng 1984); in ADHOC, we explicitly represent the plume-scale motions, and separately parameterize the SPS effects. The range of motions considered in the SPS model is larger than that considered in an LES SGS model (see Fig. 1).

It is interesting to note that SPS motion and lateral mass exchange between updrafts and downdrafts (the two challenges that we encountered in unifying MFC

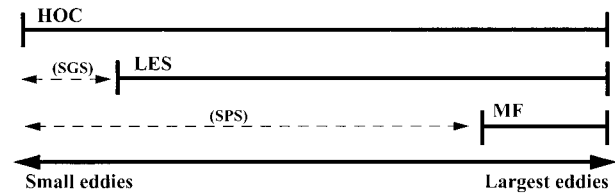


FIG. 1. Graphical interpretation of the relevant scales in HOC, LES, and mass-flux (MF) models. In order to include the effects of all scales of motion, LES models parameterize the smallest scales. In an analogous manner, ADHOC uses an SPS model to represent the part of the motion that is not represented by the tophat model.

and HOC) are in fact physically linked processes, because mixing between updrafts and downdrafts is at least in part an SPS phenomenon. However, in contrast to the issue of including SPS motions, the body of literature on entrainment and detrainment is extensive. In the next section, we will review the history of the development of these parameterizations in mass-flux models. Before we review this work, however, it is important to point out some key differences between mass exchange parameterization in a cumulus model and mass exchange in ADHOC.

In reality, the lateral mixing that occurs between updrafts and downdrafts depends on the nature of the convection. For example, in deep cumulus convection, “environmental” subsidence is slow and nonturbulent; mass-flux models were designed to represent this type of regime, while ADHOC is designed to be more general. The lateral mixing parameterization in ADHOC has the potential to handle those regimes in which both the updrafts and downdrafts are turbulent (e.g., stratocumulus regimes). The effects of mixing in a turbulent updraft will naturally be different if the mixing takes place with a nonturbulent or turbulent downdraft. Thus, in order for ADHOC to handle a wider range of PBLs, the entrainment and detrainment processes must be more general than those designed purely for cumulus parameterizations. ADHOC must include situations where the exchange is between two turbulent air masses. Additional physics must be incorporated into the system in order to 1) account for the physics of the turbulent–turbulent mass exchange and 2) distinguish between cumulus and stratocumulus cases. As we will see in section 2, ADHOC draws from HOC for this additional physics. As we will show in section 4 and in Part III of this paper (Lappen and Randall 2001b, hereafter LR3), ADHOC can in fact handle a wide range of turbulent PBLs. In the next section, we will review earlier parameterizations of entrainment and detrainment, most of which were designed specifically to address the lateral mass exchange between a turbulent updraft and a nonturbulent environment.

Review of lateral mixing parameterizations in mass-flux models

Stommel (1947) was the first to note that cumulus clouds are diluted by air from above cloud base. To our

knowledge, Batchelor (1954) made the earliest attempt to parameterize this mass exchange. He proposed that the velocities associated with lateral mixing between updrafts and downdrafts are proportional to the updraft velocity. Morton (1957), Squires and Turner (1962), and Scorer (1957) represented this mixing in terms of empirical formulas based on laboratory experiments.

Squires (1958) showed that parcels of dry air, engulfed by a cumulus cloud near cloud top, can descend a considerable distance through a cloud by entraining dry air, which evaporates and cools. Twenty years later, Telford (1975) and Raymond (1979) designed models that incorporated this concept. In contrast to the lateral entrainment models, these vertical mixing models are based on the assumption that air is incorporated into the cloud at cloud top and cloud base, and subsequently moves vertically to its level of neutral buoyancy, where it exits the cloud. The success of these models led to the concept of “buoyancy sorting” first described by Raymond and Blyth (1986, hereafter RB86).

Buoyancy sorting conceptually evolved from the observation that convective updrafts reach their level of neutral buoyancy based on undiluted ascent (Warner 1970; Heymsfield et al. 1978; Raymond and Wilkening 1982). It was proposed that cloud top would be populated by those parcels that ascended without a mixing event (RB86), suggesting that mixing takes place as a series of discrete events. Thus, RB86 generalized the conceptual model of Telford (1975) to allow mixing events throughout the depth of the cloud. They assumed that parcels of low-level air mix in varying proportions between low levels and the neutral buoyancy level for undiluted ascent. Each newly mixed subparcel then moves to its level of neutral buoyancy and detrains. The buoyancy sorting model has been refined in later studies (e.g., Taylor and Baker 1991; Kain and Fritsch 1990; Emanuel 1991).

Taylor and Baker (1991) pointed out that the problem with the RB86 model is that cloudy air detrained at its level of neutral buoyancy will become negatively buoyant upon mixing with its subsaturated environment, giving rise to additional mixing events. Emanuel (1991) recognized that in climate models, it is impractical to proceed beyond the first buoyancy sorting event. To avoid the problem envisioned by Taylor and Baker (1991), however, he assumed that air mixtures detrain at the level where their liquid water potential temperature (as opposed to their actual potential temperature) equals that of their environment. Thus, the further mixing of air with its environment will result in neutral buoyancy.

The 2D numerical experiment of Bretherton and Smolarkiewicz (1989, hereafter BS89) support the buoyancy sorting concept with one important caveat. In RB86, the cloud passively adjusts to the vertical temperature profile in the environment. BS89 argue that in order to sustain the flow of air into and out of the cloud, there must be vertical motion, and thus temperature change,

in the environment. This temperature change in the environment causes a small virtual potential temperature difference between the air that is to be detrained and the environment. BS89 show that this difference is associated with gravity waves, which cause preferential detrainment of cloud-processed air at levels where the cloud buoyancy with respect to the far environment is decreasing with height.

Most current mass-flux parameterizations for convection represent the lateral mixing terms in terms of the convective mass flux (Turner 1973; Simpson 1971; Arakawa and Schubert 1974):

$$E = \varepsilon M_c \quad \text{and} \quad D = \delta M_c. \quad (1)$$

The entrainment parameter ε is believed to be inversely proportional to the radius of the updraft R_{up} ,

$$\varepsilon = \frac{0.2}{R_{up}} \quad (2)$$

(Simpson et al. 1965; Simpson and Wiggert 1969). The detrainment parameter δ is parameterized in various ways (see later discussion).

Parameterizations for E and D that are most often employed by GCMs include that of Arakawa and Schubert (1974, hereafter AS74), Tiedtke (1989, hereafter T89), and Gregory and Rowntree (1990, hereafter GR90). AS74 defined a spectrum of “cloud types” in terms of a single parameter that was chosen to be the fractional entrainment rate λ (denoted here by ε). In view of (2), different cloud types implicitly represent updrafts of varying radii. Instead of assuming that R_{up} is constant with height, AS74 assumed that the λ for the *time-averaged* mass flux of a cloud is approximately constant with height. They assumed that clouds detrain only at their tops, which occur at their levels of neutral buoyancy. Relating detrainment to the level of neutral buoyancy became a foundation from which many parameterizations were subsequently developed (e.g., Telford 1975; Bougeault and André 1986; RB86; BS89).

Bougeault and André (1986, BA86) used a similar concept to develop a dissipation parameterization for use in HOC models. In their parameterization, the rate of dissipation of higher moments is inversely proportional to the distance to the level of neutral buoyancy of displaced parcels (or the distance to the lower boundary). This idea is explained further below.

In T89, E and D are broken down into two parts: a part that includes turbulent exchange of mass along the cloud edges and a part that accounts for organized inflow and outflow at the cloud base and the cloud top, respectively.¹ The lateral mass exchange along the cloud edges is represented as in (1) and (2). T89 assumed values for R_{up} and proposed that $\varepsilon = \delta = 10^{-4} \text{ m}^{-1}$ for

¹ Randall and Huffman (1982) argue that you cannot have organized inflow across the cloud edge without turbulent mixing, because the inflow would pinch the cloud edge, but would not actually cross into the cloud.

penetrative and midlevel convection and $\varepsilon = \delta = 3 \times 10^{-4} \text{ m}^{-1}$ for shallow convection. He also added an “enhancement” factor to increase the lateral mixing within 150 mb of cloud base. The T89 scheme is currently used in the European Centre for Medium-Range Weather Forecasts model as well as in the GCMs at the Max-Planck-Institut für Meteorologie in Hamburg and at the Bureau of Meteorology Research Centre in Melbourne, Australia. GR90, used in the Met Office GCM, is similar to T89, with the exception that δ is taken to be $\varepsilon/3$.

Recently, Siebesma and Cuijpers (1995, hereafter SC95) and Siebesma and Holtslag (1996, hereafter SH96) used LES to derive profiles of E and D . They did this for a shallow cumulus case observed during the Barbados Oceanographic and Meteorological Experiment (BOMEX). In their LES studies, SC95 and SH96 determined that the values for ε and δ used by T89 and GR90 were an order of magnitude too small. In addition, they found that $\delta > \varepsilon$. SH96 found that $\varepsilon \sim 1.5\text{--}2.5 \times 10^{-3} \text{ m}^{-1}$ and $\delta \sim 2.5\text{--}3.0 \times 10^{-3} \text{ m}^{-1}$. For the BOMEX case, they concluded that mass-flux schemes that employed T89 (or something similar) were too active.

The physical implications of the modified values of ε and δ are as follows. In T89 and GR90, both the relatively slow lateral mixing and the assumption of equal entrainment and detrainment rates imply a need for large inversion-base detrainment (mass continuity). Both the greater lateral mixing and the larger values of δ implied by SC95 and SH96 facilitate more lateral mass exchange between cloud base and the inversion base, and thus require little or no massive detrainment at the inversion. In this way, the inversion is not excessively moistened and cooled by convection. This seems reasonable for shallow cumuli because many shallow clouds do not reach the inversion at all (SH96); thus, they should completely detrain before arriving there. In summary, SH96 argue that previous values of ε and δ may be valid for penetrative and midlevel convection, but that the larger distribution of cloud types (as defined by AS74) in shallow convection prohibit the use of a single updraft radius [Eq. (2)] to describe an ensemble of these clouds. Instead, ε for an ensemble of shallow convective clouds must be calculated using a weighted average of different cloud subsets (SC95).

2. A parameterization of lateral mass exchanges for ADHOC

In ADHOC, the effects of lateral mass exchanges are represented by the E and D terms in the continuity equations [see Eqs. (21)–(22) in LR1]. In LR1, we showed that these terms are related to the dissipation terms in the higher-moment equations. In this section, we describe a new parameterization of E and D for use in ADHOC. We draw from HOC dissipation parameteri-

zations to incorporate additional physics into the mass exchange parameterization.

We base our approach on the analogy between the E and D terms in ADHOC and the dissipation terms in the HOC equations (see LR1). In order to parameterize both E and D , we need two constraints. Interestingly enough, in previous HOC models, two constraints were also used in the parameterization of dissipation. Two typical constraints are 1) a method to either diagnose or predict the dissipation timescale or length scale (e.g., Blackadar 1962; Detering and Etling 1985; Bougeault and André 1986; Beljaars et al. 1987; Canuto et al. 1994, Langland and Liou 1996), and 2) the assumption that the dissipation timescales for the different moments (i.e., fluxes, variances, triple moments) are proportional to one another (e.g., Canuto 1992; Bougeault 1981; André et al. 1978).

Mass-flux models use two constraints to parameterize E and D , but these vary depending on the scheme. For example, AS74 use 1) a constant fractional entrainment rate (for each cloud type) and 2) the assumption that detrainment occurs only at the top (where the top is the level of neutral buoyancy for air lifted from the base). RB86 use the same assumption 1, but use buoyancy sorting for the second constraint. Other studies that have applied mass-flux models to the PBL (e.g., SC95; SH96) use the two closures indicated by Eqs. (1) and (2).

As shown in LR1, the lateral mixing terms in the higher-moment equations of ADHOC are inversely proportional to the dissipation timescale used in the corresponding HOC parameterization. In the $w'w'$ equation of ADHOC, we have

$$\frac{\partial \overline{w'w'}}{\partial t} \sim -(w_{\text{up}} - w_{\text{dn}})^2 \left(\frac{E + D}{m} \right). \quad (3)$$

In HOC parameterizations, the dissipation of $\overline{w'w'}$ is written as

$$\begin{aligned} \left(\frac{\partial \overline{w'w'}}{\partial t} \right)_{\text{diss}} &= -C_1 \frac{\overline{w'w'}}{\tau} \\ &= -C_{ww} \frac{[\sigma(1 - \sigma)(w_{\text{up}} - w_{\text{dn}})^2]}{\tau}. \end{aligned} \quad (4)$$

Here, we have used the relationship

$$\overline{w'w'} = \sigma(1 - \sigma)(w_{\text{up}} - w_{\text{dn}})^2 \quad (5)$$

(see LR1 for an explanation). In (4), τ is a dissipation timescale and C_{ww} is a dissipation constant (both discussed later). In order for the ADHOC dissipation parameterization to be consistent with that used in HOC, the right-hand side of (3) must be equal to the right-hand side of (4). This implies that

$$E + D = \frac{C_{ww} m \sigma (1 - \sigma)}{\tau}. \quad (6)$$

Our method to determine τ in (6) is based on the

ideas of BA86, which we modify by incorporating some ideas from the MFC literature. By adopting the ideas of BA86, we relate E and D to the level of neutral buoyancy of displaced parcels (used by some MFC and HOC models, e.g., AS74; BA86; RB86). BA86 argued that there are two dissipation length scales: one for upward-moving parcels and one for downward-moving parcels. In order to account for the reduction of the mixing length by the effects of the inversion and the lower boundary, they chose a harmonic average of the two to obtain one dissipation mixing length that could be used to dissipate all turbulent moments:

$$\frac{1}{L_B} = \frac{1}{2} \left(\frac{1}{L_{\text{up}}} + \frac{1}{L_{\text{dn}}} \right) = \frac{1}{2} \frac{(L_{\text{up}} + L_{\text{dn}})}{L_{\text{up}} L_{\text{dn}}}, \quad (7)$$

where L_{up} and L_{dn} are defined by

$$\int_z^{z+L_{\text{up}}(z)} \beta [s_{v_{\text{parcel}}}(z'') - s_{v_{\text{enviro}}}(z'')] dz'' \equiv e(z), \quad (8)$$

$$\int_{z-L_{\text{dn}}(z)}^z \beta [s_{v_{\text{enviro}}}(z'') - s_{v_{\text{parcel}}}(z'')] dz'' \equiv e(z)(z - L_{\text{dn}} \geq 0), \quad (9)$$

and

$$\tau_B = \frac{L_B}{\sqrt{e}}. \quad (10)$$

Here τ_B is the Bougeault timescale, L_B is the total turbulent (Bougeault) length scale, L_{up} (L_{dn}) is the turbulent length scale in the upward (downward) direction, $s_{v_{\text{parcel}}}$ is the virtual static energy of a parcel lifted dry or moist adiabatically, $s_{v_{\text{enviro}}}$ is the dry static energy of the environment, e is the turbulence kinetic energy (TKE), z is height, β is the buoyancy coefficient, T_0 is a reference temperature, g is the gravitational acceleration, and C_p is the specific heat of air at constant pressure. Equations (8) and (9) say that a parcel with a given amount of TKE will adiabatically move upward or downward in an environment of a given static stability as far as it can go before its energy runs out. Of course, the distance that a parcel can move downward is also limited by the lower boundary [Eq. (9)]. By design, (7)–(9) makes L small (dissipation large) in or near statically stable layers.

Following BA86, we would like to make E and D as big as possible near the ground and the inversion, respectively, in order to accurately represent the dissipation that occurs there. With this in mind, we make the following proposal for E and D (our two constraints) in ADHOC:

$$E = \frac{C_{\text{ww},E} \sigma(1 - \sigma) M_c}{L_{\text{dn}}} \quad \text{and} \quad (11)$$

$$D = \frac{C_{\text{ww},D} \sigma(1 - \sigma) M_c}{L_{\text{up}}}.$$

Here $C_{\text{ww},E}$ and $C_{\text{ww},D}$ are two different constants related to entrainment and detrainment, respectively (this will be explained more below). In (11), we use a slightly modified version of (8) and (9) to determine L_{up} and L_{dn} ; we replace s_v with $s_{v_{\text{up}}}$ in (8) and $s_{v_{\text{dn}}}$ in (9) so that the upward (downward) length scale is determined using the updraft (downdraft) sounding instead of the mean-state sounding. Note that in order to satisfy (6), we must add the expressions for E and D in (11). This gives an expression that is proportional to the BA86 HOC length scale parameterization [Eq. (7)]. We would get a similar result if L_{up} and L_{dn} were interchanged in (11). However, in the latter case, detrainment would be large near the ground (where L_{dn} is small), while entrainment would be large near the inversion, the opposite of what occurs.

If we temporarily assume that $C_{\text{ww},E} = C_{\text{ww},D} \equiv C_{\text{ww}}$, and we plug (11) into (6), we get

$$E + D = \frac{C_{\text{ww}} M_c \sigma(1 - \sigma)}{L_B}. \quad (12)$$

The parameterization given by (11) then reduces to the assumption that

$$\tau_B = \frac{L_B}{M_c/m} = \frac{L_B}{\sigma(1 - \sigma)(w_{\text{up}} - w_{\text{dn}})}. \quad (13)$$

If we compare (13) to the Bougeault parameterization (10), we see that the relevant velocity scale in ADHOC (with $C_{\text{ww},E} = C_{\text{ww},D} \equiv C_{\text{ww}}$) is M_c/m . This plays the role of the turbulent velocity scale \sqrt{e} in Bougeault's parameterization.

We must now choose the values of $C_{\text{ww},E}$ and $C_{\text{ww},D}$. We know that the mass flux in a convective boundary layer (CBL) is a maximum [$(\partial M_c / \partial z) = 0$] at roughly $z/z_i = 0.4$ (Willis and Deardorff 1974; André et al. 1976). Thus, at this height, we can write

$$E - D = \sigma(1 - \sigma) M_c \left(\frac{C_{\text{ww},E}}{L_{\text{dn}}} - \frac{C_{\text{ww},D}}{L_{\text{up}}} \right) = 0. \quad (14)$$

In the middle of the CBL, neither $\sigma(1 - \sigma)$ nor M_c is equal to zero. It follows that

$$\frac{C_{\text{ww},E}}{L_{\text{dn}}} - \frac{C_{\text{ww},D}}{L_{\text{up}}} = 0 \quad \text{at} \quad \frac{z}{z_i} = 0.4. \quad (15)$$

Due to the near-neutral stratification of the CBL, the upward and downward length scales that result from turbulent mixing will extend to the PBL top and surface, respectively. Thus, at $z/z_i = 0.4$ the ratio of these two length scales is $L_{\text{up}}/L_{\text{dn}} = 3/2$. Using this in (15), we get

$$\frac{C_{\text{ww},D}}{C_{\text{ww},E}} = \frac{3}{2}. \quad (16)$$

In order to choose the values of $C_{\text{ww},E}$ and $C_{\text{ww},D}$, we built a ‘‘toy’’ model of a cloud-free convective boundary layer. This model is described in the appendix. Using previously established similarity relationships in this

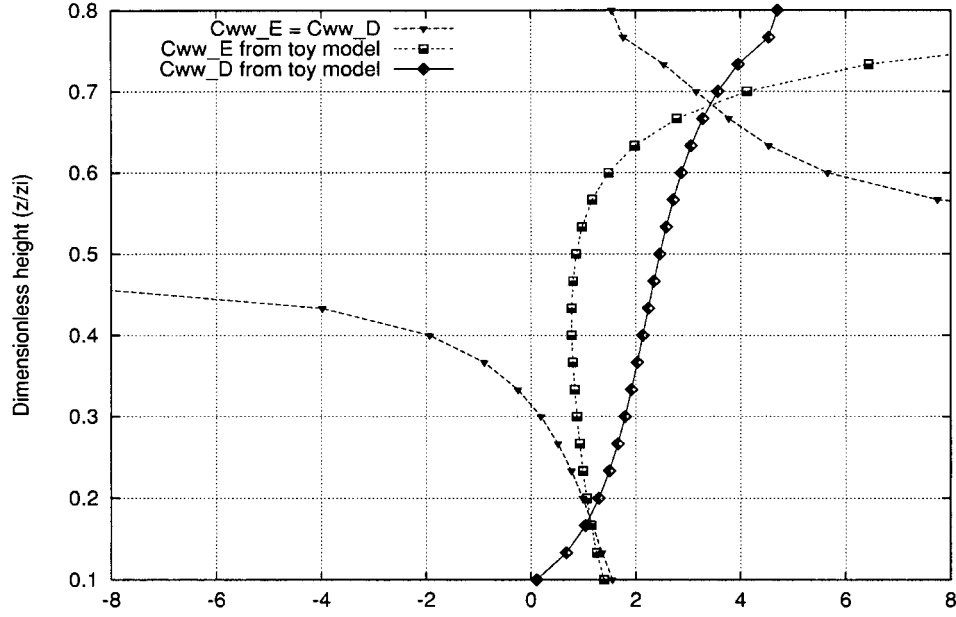


FIG. 2. Entrainment and detrainment constants $C_{ww,E}$ and $C_{ww,D}$ as determined by a toy model of cloud-free convection. For reference, we show the profile for $C_{ww,E} = C_{ww,D}$.

model, we were able to derive profiles of $C_{ww,E}$ and $C_{ww,D}$. The results are plotted in Fig. 2. In the interior of the PBL (where the similarity relationships are valid), both constants are of order one, with $C_{ww,D}$ larger than $C_{ww,E}$. The ratio of $C_{ww,D}/C_{ww,E}$ is between 1.0 and 2.5 [consistent with Eq. (16)]. Since we know from Fig. 2 that the magnitudes of these constants are of order one, we choose

$$C_{ww,D} = 1.5 \quad \text{and} \quad C_{ww,E} = 1.0. \quad (17)$$

As will be shown, these values perform quite well over a range of PBLs from trade wind cumulus (shown below) to marine stratocumulus and dry convection (shown in LR3).

If we substitute (11) and (17) into (3), we get the following final form for the lateral mass exchange terms in the $w'w'$ equation:

$$\frac{\partial \overline{w'w'}}{\partial t} \sim -(w_{up} - w_{dn})^2 \sigma (1 - \sigma) \frac{M_c}{m} \left(\frac{C_{ww,E}}{L_{dn}} + \frac{C_{ww,D}}{L_{up}} \right). \quad (18)$$

Using (5), we can write this as

$$\frac{\partial \overline{w'w'}}{\partial t} \sim -\overline{w'w'} \frac{M_c}{m} \left(\frac{C_{ww,E}}{L_{dn}} + \frac{C_{ww,D}}{L_{up}} \right). \quad (19)$$

In (19), M_c and the bracketed terms are always positive, and thus the parameterization for E and D will always act to dissipate $w'w'$.

Since E and D represent the process of mass transfer into and out of a turbulent updraft, respectively (as opposed to representing the dissipation of a specific moment), we must use the parameterization given by (11)

in all of the ADHOC equations. The final form for the parameterization of these terms in the triple-moment equation, $w'w'w'$, is

$$\begin{aligned} \frac{\partial \overline{w'w'w'}}{\partial t} &\sim -(w_{up} - w_{dn})^3 \sigma (1 - \sigma) \\ &\times \frac{M_c}{m} \left[(2 - 3\sigma) \frac{C_{ww,E}}{L_{dn}} + (1 - 3\sigma) \frac{C_{ww,D}}{L_{up}} \right] \end{aligned} \quad (20)$$

(see LR1). Using the ADHOC relation

$$\overline{w'w'w'} = \sigma (1 - \sigma) (1 - 2\sigma) (w_{up} - w_{dn})^3, \quad (21)$$

we can write (20) as

$$\begin{aligned} \frac{\partial \overline{w'w'w'}}{\partial t} &\sim -\overline{w'w'w'} \frac{M_c}{m} \left[\frac{(2 - 3\sigma) C_{ww,E}}{(1 - 2\sigma) L_{dn}} + \frac{(1 - 3\sigma) C_{ww,D}}{(1 - 2\sigma) L_{up}} \right]. \end{aligned} \quad (22)$$

The parameterization given by (22) will act to dissipate $w'w'w'$, although this effect is not as obvious as that in (19). Such behavior is not too surprising though because we know that entrainment and detrainment modify σ directly, and that $[m\sigma(1 - \sigma)(1 - 2\sigma)(w_{up} - w_{dn})^3]$ is closely related to σ [see Eq. (10) in LR1]. Very roughly, we see that an increase in the mass flux (M_c) or a decrease in either turbulent length scale (L_{up} or L_{dn}) will increase the rate of dissipation of $w'w'w'$. However, the role of the σ coefficients inside the brackets is not that obvious. Since M_c , L_{up} and L_{dn} are all positive, the sign

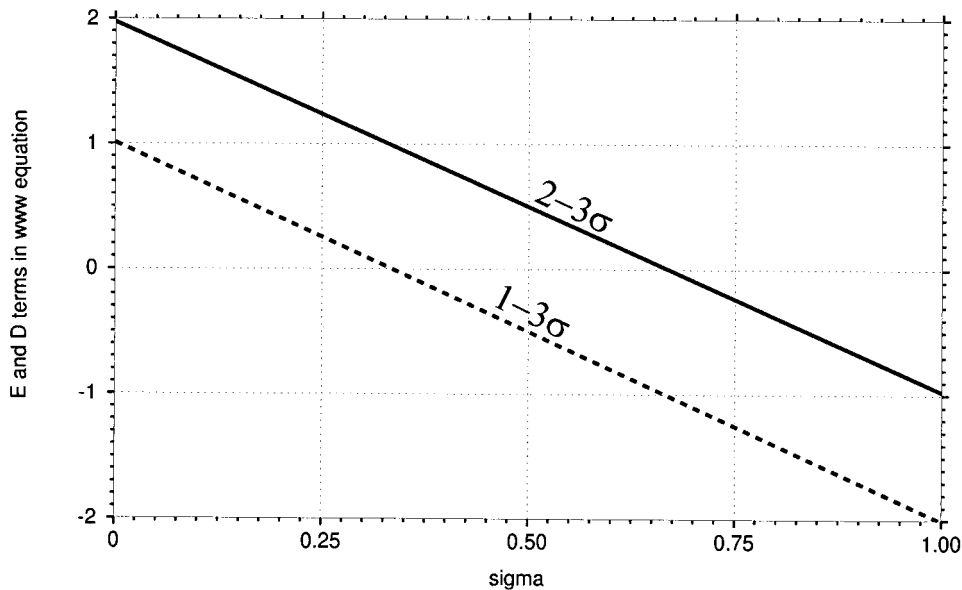


FIG. 3. The horizontal axis is sigma. The upper and lower slanting lines are plots of $2-3\sigma$ and $1-3\sigma$, respectively.

of these σ expressions will determine the ultimate sign of this dissipation term. When $w'w'w'$ is large and *positive*, σ is small [convective regime; see Eq. (10) in LR1], and both σ expressions in (22) are positive. This is true for $\sigma < 1/3$ (see Fig. 3). Thus, for this range of σ , the parameterization will act to dissipate a large positive $w'w'w'$. When $w'w'w'$ is large and *negative* (large σ), both of the σ expressions in (22) are positive. Since $w'w'w'$ is negative now, the right-hand side of (22) will be positive and will act to dissipate the negative $w'w'w'$ (push it toward zero). This is true for all $\sigma > 2/3$ (see Fig. 3). Finally, we see that when $\sigma = 1/2$, the dissipation of $w'w'w'$ is instantaneous. Our parameterization thus guarantees that $w'w'w' = 0$ for $\sigma = 1/2$. This is exactly what should happen [see Eq. (21)].

For σ in the range $1/3 < \sigma < 2/3$ (excluding $\sigma = 1/2$), it is a little less clear whether (22) truly acts as a dissipation term. Let us examine this in more detail. If $1/3 < \sigma < 1/2$, we would expect narrow updrafts and a positive $w'w'w'$. This situation, which is indicative of strong surface-driven convection, has an L_{up} , which extends to the PBL top (BA86). Since L_{dn} is always small near the ground, the first σ term in (22) will have the larger effect. This term is positive for $1/3 < \sigma < 2/3$. This, along with the negative sign in front of the right-hand side of (22), implies that the positive $w'w'w'$ will be dissipated. A similar argument can be used for the range $1/2 < \sigma < 2/3$. Based on this discussion, it appears as if the parameterization shown by (22) will act to dissipate $w'w'w'$ over the full range of σ .

The parameterization given by Eq. (11) can be compared to that most commonly used in mass-flux models, Eq. (1). The parameterizations given by (11) and (1) are equivalent if

$$\varepsilon = \frac{C_{wwE}\sigma(1-\sigma)}{L_{dn}} \quad \text{and} \quad \delta = \frac{C_{wwD}\sigma(1-\sigma)}{L_{up}}. \quad (23)$$

Comparison of (23) and (2) shows that L_{up} and L_{dn} are related to the updraft radius. Thus, these length scales may give information on the aspect ratio of the cloud. In most mass-flux models that use Eq. (1), ε and δ are constants whose magnitudes change depending on the regime being simulated [SC95; a notable exception for deep convection is Kain and Fritsch (1990)]. In ADHOC, we see that ε and δ are functions of σ , L_{up} , and L_{dn} , which are functions of height. Setting ε and δ equal to constants means that the fractional entrainment and detrainment rates are constant with height. While this may provide good estimates of E and D in some regimes, Eq. (11) allows E and D to depend on the situation, which is more physical. For example, when the downdraft (updraft) turbulent length scale is small, the ADHOC parameterization shows that entrainment (detrainment) will become large. This is consistent with large detrainment at the neutral buoyancy level (small L_{up}). This physically observable result cannot be duplicated by setting ε and δ equal to constants.

For a 1-km deep dry convective boundary layer, typical ADHOC values of ε and δ are given in Table 1. These values are in the same range as those previously proposed (e.g., SC95, $\varepsilon = 3 \times 10^{-3} \text{ m}^{-1}$ and $\delta = 4 \times 10^{-3} \text{ m}^{-1}$; GR90, $\varepsilon = 4 \times 10^{-4} \text{ m}^{-1}$ and $\delta = 1.3 \times 10^{-4} \text{ m}^{-1}$). SC95 showed using BOMEX data that the overall fractional detrainment rate δ must be larger than the overall fractional entrainment rate ε . For the dry PBL values shown in Table 1, ADHOC agrees with this result near the inversion. Near the surface, however, ADHOC shows the opposite ($\varepsilon > \delta$). Figure 4 shows

TABLE 1. Typical values for the fractional entrainment rates in ADHOC.

	σ	L_{up}	L_{down}	ϵ	δ
Near the surface	0.5	1000 m	10 m	2.5×10^{-2}	3.75×10^{-4}
Near the inversion	0.3	100 m	900 m	1.0×10^{-4}	1.35×10^{-3}
At the inversion	0.5	10 m	1000 m	2.5×10^{-4}	3.75×10^{-2}

profiles of ϵ and δ simulated by ADHOC for BOMEX (the BOMEX case setup is discussed in section 4). The typical values found by both SC95 and GR90 (for the cloudy region only; 600–1500 m) are also shown for reference. We see the height dependence of the ADHOC formulas. In the lower part of the cloud, ADHOC agrees with the value used by SC95. Near cloud top, the ADHOC formulas allow for the fractional entrainment/detrainment rates to increase. The ADHOC results support the SC95 assertion that the formulas used by GR90 (for both ϵ and δ) are an order of magnitude too small.

In section 4, we show profiles of E and D from a simulation of shallow cumulus observed during BOMEX. We compare these profiles to those of SC95. First, however, we will describe another new parameterization used in ADHOC—a method to include the SPS fluxes.

3. The subplume-scale fluxes

As discussed in section 1, although SPS motions have never been explicitly represented in *either* MFC or HOC models, the importance of their effects becomes appar-

ent when the two theories are unified. In ADHOC, we combine in one set of equations MFC (an inherently LES) with HOC (a scheme that is supposed to represent all scales of motion). In order to combine these two approaches so that the equations are consistent scale-wise, there is a need to add SPS motions to the mass-flux equations to obtain realistic results in regions where the motions are inherently small scale (e.g., near the surface and the inversion). Figure 1 qualitatively depicts the relevant SPS eddy size in ADHOC. In section 4, we will show that, without the SPS parameterization, ADHOC is unable to realistically simulate the entrainment rate (near the inversion) and the in-cloud and near-surface turbulence in BOMEX.

In ADHOC, the SPS effects are included in generic source/sink terms, which appear in both the mean-state and turbulent flux equations. In LR1, we derived these equations for an arbitrary thermodynamic variable h (\bar{h} and $\overline{w'h'}$, respectively). In these equations, the terms that represent the sources/sinks of h (S_h) are

$$\frac{\partial}{\partial t} m \bar{h} \sim m \overline{(S_h)} \quad \text{and} \quad (24)$$

$$\frac{\partial}{\partial t} \overline{m w' h'} \sim M_c [(S_h)_{\text{up}} - (S_h)_{\text{dn}}], \quad (25)$$

where $\overline{(S_h)}$ represents the divergence of the SPS flux in (24), and the SPS contribution to the tendency of $\overline{w'h'}$ (among other things) in (25). We can write the contribution to the mean state as

$$\frac{\partial}{\partial t} m \bar{h} \sim -\frac{\partial}{\partial z} (\overline{m w' h'}_{\text{sp}}), \quad (26)$$

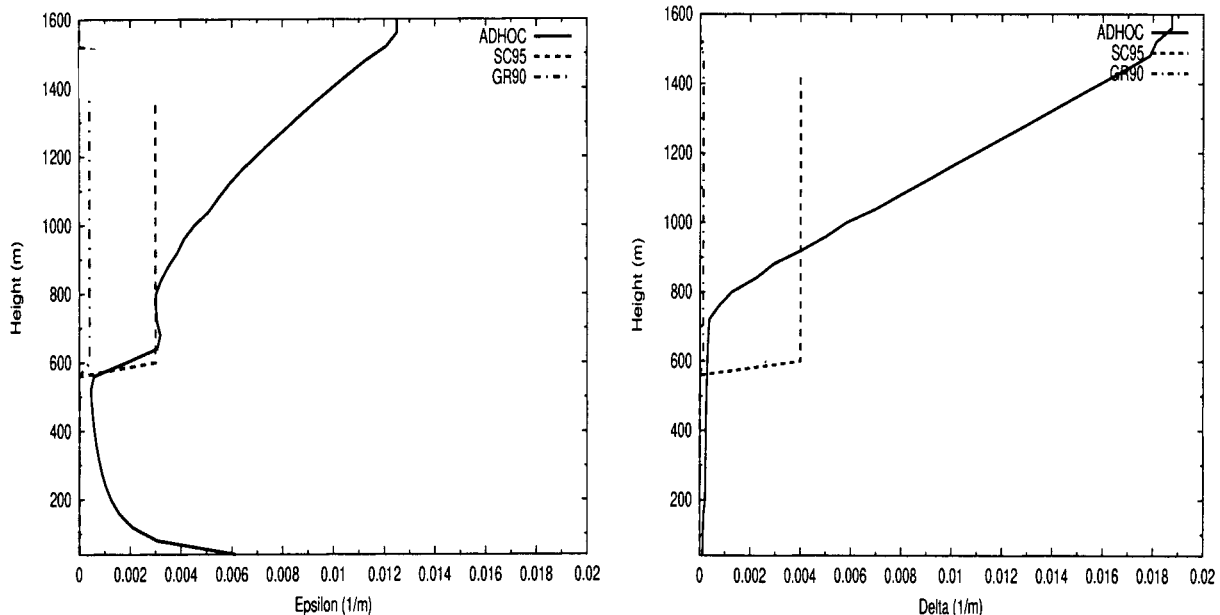


FIG. 4. The implied fractional entrainment (ϵ) and detrainment (δ) rates simulated by ADHOC [calculated from Eq. (23)]. The dashed line is the value derived by SC95 for BOMEX; the dot-dashed line is that used by GR90.

and if we assume that these SPS fluxes are downgradient (a valid assumption for small eddies), we can write the contribution to the flux as

$$\frac{\partial}{\partial t} \overline{m w' h'} \sim \frac{M_c}{\sigma} \frac{\partial}{\partial z} \left(K_h \sigma \frac{\partial \bar{h}}{\partial z} \right)_{\text{up}} - \frac{M_c}{(1 - \sigma)} \frac{\partial}{\partial z} \left[K_h (1 - \sigma) \frac{\partial \bar{h}}{\partial z} \right]_{\text{dn}}, \quad (27)$$

where the subscript ‘‘up (dn)’’ denotes an updraft (downdraft) quantity, and K_h is the SPS eddy diffusivity for heat (different for the updrafts and downdrafts). The *area-averaged* SPS eddy flux appears in the mean-state equation, while the updraft and downdraft SPS fluxes appear separately in the second-moment equation.

To parameterize the SPS fluxes, we use a modified version of the subgrid-scale turbulence energy model proposed by Deardorff (1980),

$$\frac{\partial e_{\text{sps}}}{\partial t} = -\overline{w' u'}_{\text{sps}} \frac{\partial U}{\partial z} - \overline{w' v'}_{\text{sps}} \frac{\partial V}{\partial z} + \frac{g}{C_p T_0} \overline{w' s'_{v\text{sps}}} - \frac{\partial}{\partial z} [\overline{w' (e_{\text{sps}} + p' / \rho_0)}] - \varphi_{\text{sps}} = \varphi_{\text{ls}}, \quad (28)$$

where e_{sps} is the SPS TKE, U and V are the mean wind components, p is the pressure, ρ_0 is a reference density, s_{sps} is the rate of dissipation of SPS TKE, and s_{ls} is the large-scale dissipation rate. We evaluate the SPS TKE separately for the updrafts and downdrafts. This is particularly important in regions of partial cloudiness (e.g., shallow cumuli), where we expect the SPS turbulence to be stronger in the cloudy updrafts and weaker in the clear downdrafts. The large-scale dissipation of TKE (s_{ls}) acts as a *source* of SPS TKE. We thus assume that the large-scale TKE is not directly dissipated, but cascades from the large to the small (SPS) scales (Kolmogorov 1942). We feed the surface fluxes directly into the large scale, and due to a large near-surface dissipation rate (small dissipation length scale), the SPS energy quickly grows and dominates that of the large scale.

We close (28) using the downgradient diffusion assumption

$$\overline{[w' (e_{\text{sps}} + p' / \rho_0)]} = -2K_m \frac{\partial \bar{e}_{\text{sps}}}{\partial z} \quad (29)$$

and the Kolmogorov hypothesis

$$\varepsilon_{\text{sps}} = \frac{C(\bar{e}_{\text{sps}})^{1.5}}{l}, \quad (30)$$

where

$$C = 0.19 + 0.51 \frac{l}{\Delta z} \quad (31)$$

[we adjust the value of C to 3.9 at the lowest layer due to wall effects (Deardorff 1980)], Δz is the vertical grid spacing, and l is a length scale specified as

$$l = \Delta z \quad (32)$$

when the stratification is unstable, and

$$l = 0.76 \left(\frac{\bar{e}_{\text{sps}}}{\left(\frac{g}{C_p T_0} \frac{\partial s_v}{\partial z} \right)} \right)^{1/2} \quad (33)$$

when the stratification is stable. In the latter case, we impose an upper limit of $l = \Delta z$.

Finally, we calculate the eddy diffusivities for momentum and heat using

$$K_m = 0.1l(\bar{e}_{\text{sps}})^{1/2} \quad \text{and} \quad K_h = \left(1 + 2 \frac{l}{\Delta z} \right) K_m, \quad (34)$$

and use these to calculate $\overline{w' u'}_{\text{sps}}$ and $\overline{w' v'}_{\text{sps}}$ (using a downgradient assumption). In order to calculate $\overline{w' s'_{v\text{sps}}}$, we write it in terms of the SPS fluxes of liquid water static energy $\overline{w' s'_{L\text{sps}}}$ and total water mixing ratio $\overline{w' r'_{T\text{sps}}}$ (Randall 1987). The latter two quantities are calculated using a downgradient assumption, with the eddy diffusivity for heat given by Eq. (34). We also need to calculate $\overline{w' w'}_{\text{sps}}$ separately for updrafts and downdrafts in order to evaluate the source terms discussed in LR1 [see Eq. (40) of LR1]. Since small-scale turbulence tends to be isotropic, we assume equipartitioning of the three components ($\overline{u' u'}_{\text{sps}}$, $\overline{v' v'}_{\text{sps}}$, and $\overline{w' w'}_{\text{sps}}$) of the prognosed SPS TKE, thus

$$\overline{w' w'}_{\text{sps}} = \frac{2}{3} e_{\text{sps}}. \quad (35)$$

The above calculations are done separately for the updraft and downdraft, as required for the prognostic higher-moment equations (see LR1). In order to time step Eq. (28) separately for the updraft and downdrafts, we must decide how to partition (between the updrafts and downdrafts) both the large-scale dissipation rate [which is a source term for the SPS TKE in Eq. (28)] and the mean winds (U and V). In partitioning these quantities, we must ensure that the sum of the area-weighted updraft and downdraft values adds up to the total. With this in mind, we choose

$$U_{\text{up}} = U_{\text{dn}} = U \quad \text{and} \quad (36)$$

$$\varepsilon_{\text{up}} = \frac{\varepsilon}{2\sigma}; \quad \varepsilon_{\text{dn}} = \frac{\varepsilon}{2(1 - \sigma)}. \quad (37)$$

The reason for using (37) instead of a simpler form analogous to (36) is that (37) allows stronger (weaker) dissipation in the updraft when σ is small (big). Mass continuity dictates that when σ is very small, the updraft speed is faster than that of the downdraft; this implies stronger turbulence and stronger dissipation. The procedure for incorporating the SPS contribution into the mean-state equations [see Eq. (26)] is somewhat easier. It requires the *total* SPS flux, which is obtained using

$$\overline{(w' x')_{\text{sps}}}_{\text{Total}} = \sigma \overline{(w' x')_{\text{sps}}}_{\text{up}} + (1 - \sigma) \overline{(w' x')_{\text{sps}}}_{\text{dn}}. \quad (38)$$

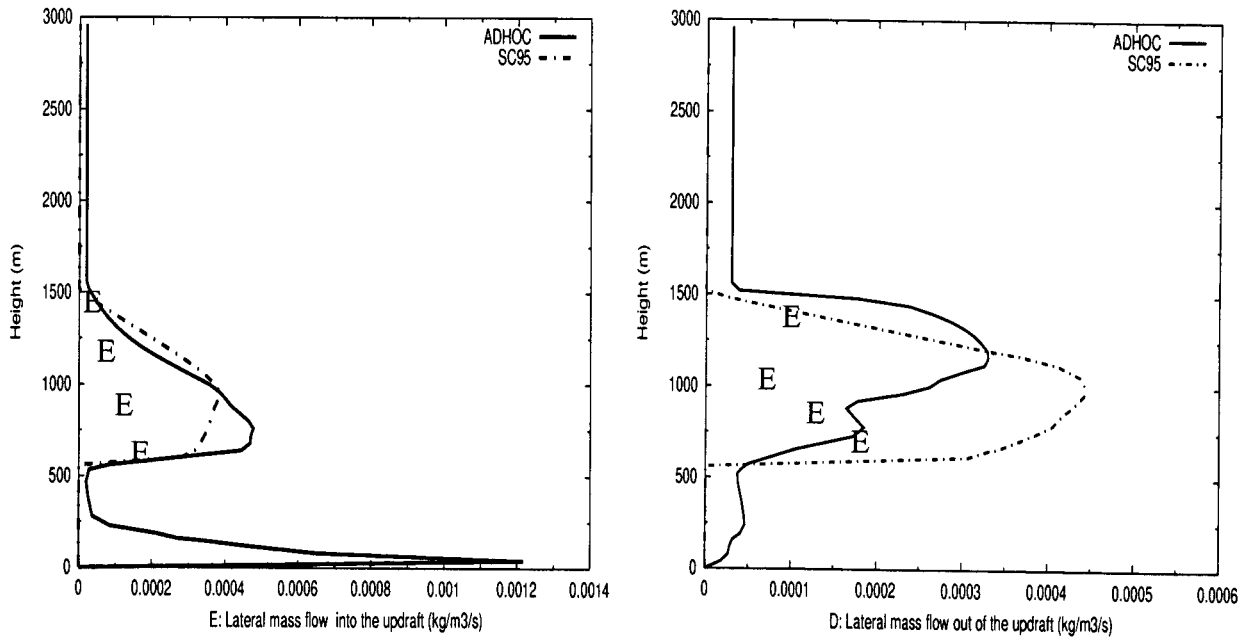


FIG. 5. Comparison of the lateral mass exchange rates into and out of the updraft simulated by ADHOC with those diagnosed by ADHOC using the SC95 parameterization. The E's are from Esbensen (1978), based on BOMEX data.

In the next section, we show results from BOMEX in which we demonstrate the importance of including the SPS effects in ADHOC.

4. Tests with a trade wind cumulus case

a. BOMEX case description

BOMEX took place on 22–30 June 1969 near Barbados. It was designed to study the atmospheric trade wind regime and its associated cloudiness. During the study, the conditions evolved from an “undisturbed” to a “disturbed” period. The undisturbed period (used in this study, 22–26 June 1969) was characterized by downward motion below 500 mb, an apparent heat sink and moisture source near the top of the inversion (located near 800 mb), and a substantial small-scale eddy moisture flux confined below the inversion. The heat budget during this phase was dominated by radiative cooling and a surface sensible heat flux. Approximately two-thirds of the sensible heat input at the surface was lost through radiation and the rest heated up the mixed layer. The sensible heat flux at the top of the mixed layer is small during the undisturbed period. The moisture budget during this period is dominated by a balance between the incoming surface latent heat flux and the entrainment drying at the mixed-layer top. Less than 10% of the flux is used to moisten the mixed layer. During this period, cloud fraction was approximately 20%.

We ran this case using the computational design outlined by the Global Energy and Water Cycle Experiment (GEWEX) Cloud System Studies (GCSS; Browning 1994)

boundary layer cloud working group IV. The GCSS boundary layer cloud working group aims to improve physical parameterizations of clouds and other boundary layer processes and their interactions. To achieve this, the GCSS group designs intercomparison studies between observational or laboratory case studies and a wide variety of boundary layer models. The BOMEX GCSS trade wind cumulus case was set up by P. Siebesma of the Royal Netherlands Meteorological Institute (KNMI). For this intercomparison study, the BOMEX undisturbed period from 22 to 26 June was chosen (additional information available online at <http://www.knmi.nl/~siebesma/bomex.html>). A summary of the initial conditions, the large-scale forcing, and the model specifics for this case can be found there.

The results here focus only on the two new ADHOC parameterizations discussed in sections 2 and 3. They are compared with LES results. The LES models used for comparison in this study are from the University of California, Los Angeles (Stevens et al. 1996), KNMI (Cuijpers and Duynkerke 1993), and the National Center for Atmospheric Research (NCAR; Moeng 1984). More general results from this case are shown in LR3, along with a more complete discussion of the trade wind regime.

b. Results and discussion

In this section, we use results from a simulation of BOMEX to demonstrate the effectiveness of the parameterizations discussed in sections 2 and 3. Figure 5 shows the ADHOC-simulated values for E and D , along

with those diagnosed by ADHOC using the SC95 formulas [Eq. (1) with $\varepsilon \sim 1.5 - 2.5 \times 10^{-3} \text{ m}^{-1}$ and $\delta \sim 2.5 - 3.0 \times 10^{-3}$], and those obtained by Esbensen (1978) by applying a cloud model to the BOMEX data. In ADHOC, mass is exchanged between the updraft and downdraft at all levels, while in SC95, the entrainment and detrainment parameterizations are used only within the cloud. Due to the dependence on the turbulent length scales [L_{up} and L_{dn} ; see Eq. (11)], the ADHOC-simulated E is large in the lower part of the boundary layer (small L_{dn}), while D is small (large L_{up}). The ADHOC profiles for E and D make physical sense (qualitatively) in that we expect E to be a maximum near the surface, where air enters the updraft, and D to be a maximum near cloud top, where air enters the downdraft. The simulated E and D profiles are in qualitative agreement with those found by Lin and Arakawa (1997) for deep convection.

In the cloud, ADHOC and SC95 produce roughly the same value for E . The maximum in ADHOC is near cloud base (where the heating as a result of latent heat release likely drives mixing into the updraft), while the maximum in SC95 is a little higher (at the location of the mass-flux maximum). Both show a steady decrease to zero from the middle to the top of the cloud. The E profile of Esbensen (1978) agrees qualitatively with the parameterized profiles, but is smaller in magnitude. There is more difference between the two parameterizations for D in the cloud. Here, ADHOC shows a maximum near the inversion and a secondary maximum near cloud base, while SC95 has a single maximum roughly in the middle of the cloud. The location of the ADHOC maximum is a direct result of the dependence on D of L_{up} [see Eq. (11)], while the location of the SC95 maximum is coincident with the location of the mass-flux maximum. In the SC95 parameterization, D is always larger than E by a constant factor. With this assumption, the SC95 curve for D agrees with that of ADHOC in the upper one-third of the cloud, but is larger in the lower two-thirds. Like ADHOC, the results of Esbensen (1978) clearly show two maxima, although in contrast to ADHOC, the larger maximum is at cloud base.

Part of the difference between the ADHOC curves and those of SC95 (in the cloud) is a result of the different height dependence of the fractional entrainment and detrainment rates in these models (shown in Fig. 4). A large amount of the difference however, is the result of the different definitions for the convective mass flux that are used in ADHOC and in SC95. In SC95, a cloud-environment decomposition is used. With this decomposition, although the vertical velocity increases with height, the mass flux *decreases* with height because the cloud fraction decreases with height. Thus, by continuity, D must be larger than E [see Eq. (47) in LR1]. In ADHOC, M_c *increases* with height in the lower part of the cloud; thus, E is larger than D .

The ADHOC formulation has the advantage that it can be applied to all turbulent masses, whether or not an organized updraft or clouds are present. The SC95

formulas are relationships that were specifically derived (from an LES) for shallow cumulus convection. The difference is subtle but significant; in ADHOC, E and D are not truly “entrainment” and “detrainment” in the classic cumulus-parameterization sense; they represent mass flow across the edge of a turbulent mass rather than mass flux across an updraft edge (in the case of shallow cumulus convection, these two regions coincide; however, the ADHOC formulas can be applied even if this is not the case). As shown below and in LR3, the ADHOC formulation works well for a variety of PBL regimes, including BOMEX.

In Figs. 6 and 7, we show results from BOMEX that demonstrate the importance of the SPS turbulence. As discussed, we would expect the impact of the SPS parameterization to be largest in regions where the dominant eddies are smallest (i.e., near the surface and near the inversion). For BOMEX, we would expect the SPS turbulence to help mix the relatively dry and warm inversion air into the cloud, decreasing both liquid water content and the in-cloud turbulence. We would also expect the SPS turbulence near the surface to help mix the subcloud layer by increasing the near-surface turbulent mixing.

Figure 6 shows the ADHOC- and LES-simulated mean-state liquid water potential temperature and mixing ratio for BOMEX after steady state is reached. The ADHOC results are shown for simulations done with and without the use of an SPS scheme. Both with and without the effects of SPS turbulence, ADHOC is able to capture the three-layer structure that is typical of the trade wind regime (the lower well-mixed subcloud layer, the conditionally unstable cloud layer, and the stable inversion layer). For the mean liquid water potential temperature, the main difference between the two simulations occurs in the subcloud layer. We see that without the SPS turbulence, the subcloud layer is too cold. The addition of SPS motion enables stronger mixing, which allows the subcloud layer to warm up to the values simulated by the LES. For the liquid water mixing ratio, we see that the cloud layer is significantly drier and closer to the values simulated by LES with the SPS turbulence scheme. As was discussed in the BOMEX GCSS working group I workshop (P. Siebesma 1997, personal communication), single-column models tend to produce 5–10 times as much liquid water as that produced by LES for BOMEX. ADHOC has only about three times too much with the SPS scheme turned on. No observational data on liquid water mixing ratio are available.

Figure 7 shows the ADHOC-simulated total water flux, virtual and liquid water potential temperature fluxes, and the vertical momentum variance for runs done both with and without the inclusion of SPS motion. For comparison, we also show the LES-simulated fields.² In

² The NCAR LES results are noisier than the others because they are averaged only for a limited number of realizations.

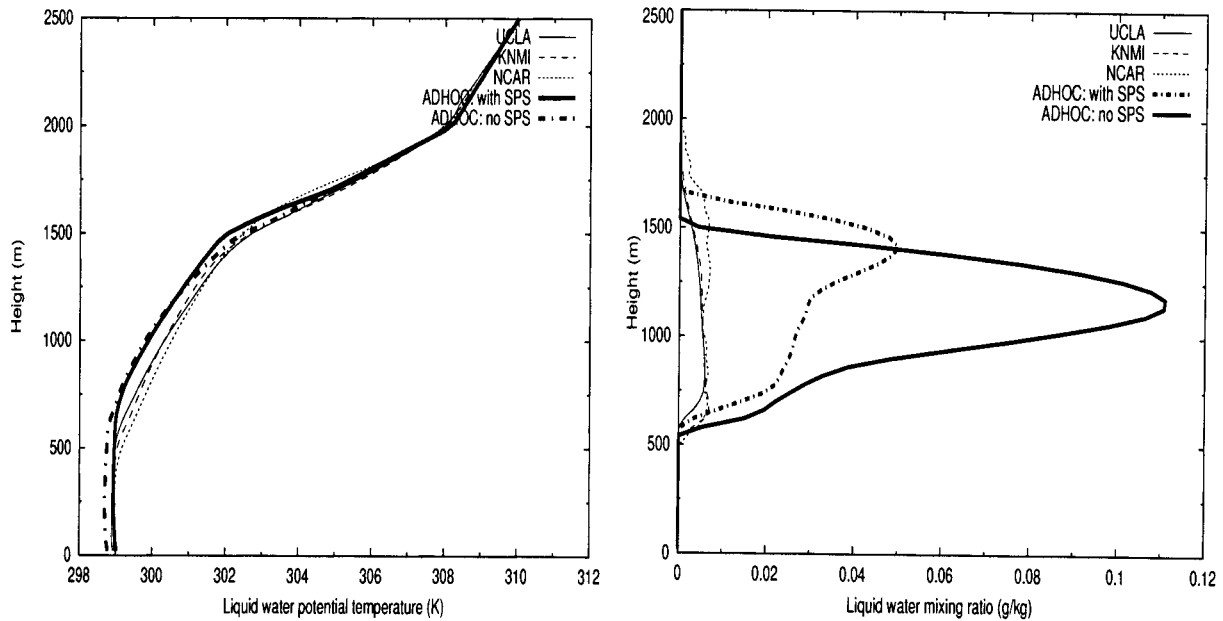


FIG. 6. Comparison of the ADHOC-simulated liquid water potential temperature and liquid water mixing ratio (for runs done with and without the inclusion of SPS motions) to those simulated by LES.

all four cases, the ADHOC results are closer to those of the LES with the SPS scheme included. The biggest differences between the two ADHOC runs occur in the cloud and near the surface, the exact regions where we would expect the SPS motion to have the greatest impact.

In summary, the SPS fluxes act to 1) increase mixing in the subcloud layer and 2) dry out the cloud layer, decreasing the in-cloud turbulence. Without the small-eddy fluxes, the mass-flux model is unable to capture the turbulent or mean structure of the BOMEX atmosphere.

5. Summary and conclusions

In this paper, we outlined a new parameterization that can be used to represent the lateral mass exchange terms in mass-flux and other plume-based atmospheric models. This parameterization is based on the idea that the lateral mass exchange terms (E and D) are directly analogous to the dissipation terms in the corresponding “standard” HOC equations (as shown in LR1). Since ADHOC combines the ideas of MFC and HOC, we have drawn from both fields in developing this parameterization. We use Bougeault’s dissipation timescale from the HOC literature, and the idea that entrainment and detrainment are related to the level of neutral buoyancy of mixed parcels employed by both MFC (AS74; RB86) and HOC (BA86).

We base our approach on the differing forms that the E and D terms take in the second- and third-moment equations, and we equate these forms to the corresponding forms of the dissipation terms in HOC parameter-

izations. We have shown that the resulting parameterization is able to capture the physics of shallow cumulus convection (in LR3, we also show this for dry convection and stratocumulus). It is the additional physics incorporated by HOC that allows this parameterization to be more general than those previously designed for studying only cumulus convection in mass-flux models (e.g., SC95; Simpson 1971).

Another new feature of ADHOC is the inclusion of the effects of SPS motion. With the SPS scheme in ADHOC, we are able to account for the portion of the turbulent motion, which is not represented with the “tophat” PDF. It has been shown in several studies that the tophat contribution to fluxes and variances represents only a fraction of the total (Businger and Oncley 1990; Young 1988; Schumann and Moeng 1991; Wyngaard and Moeng 1992; de Laat and Duynkerke 1998; SC95). Recently, Petersen et al. (1999) and Wang and Stevens (2000) showed that the missing contribution comes from SPS motions.

The current study is the first attempt to actually implement an SPS parameterization in a mass-flux model to account for the motions that the tophat PDF is unable to capture. The SPS terms appear in both the mean state and the flux equations [Eqs. (26)–(27)]. To parameterize the SPS fluxes, we use a modified version of the subgrid-scale turbulence energy model proposed by Deardorff (1980) in which the large-scale energy dissipation is a source term for the SPS motion. Due to the form that the SPS contribution takes in the flux equations [Eq. (27)], we calculate these effects separately for the updrafts and downdrafts.

We presented results from the simulation of trade

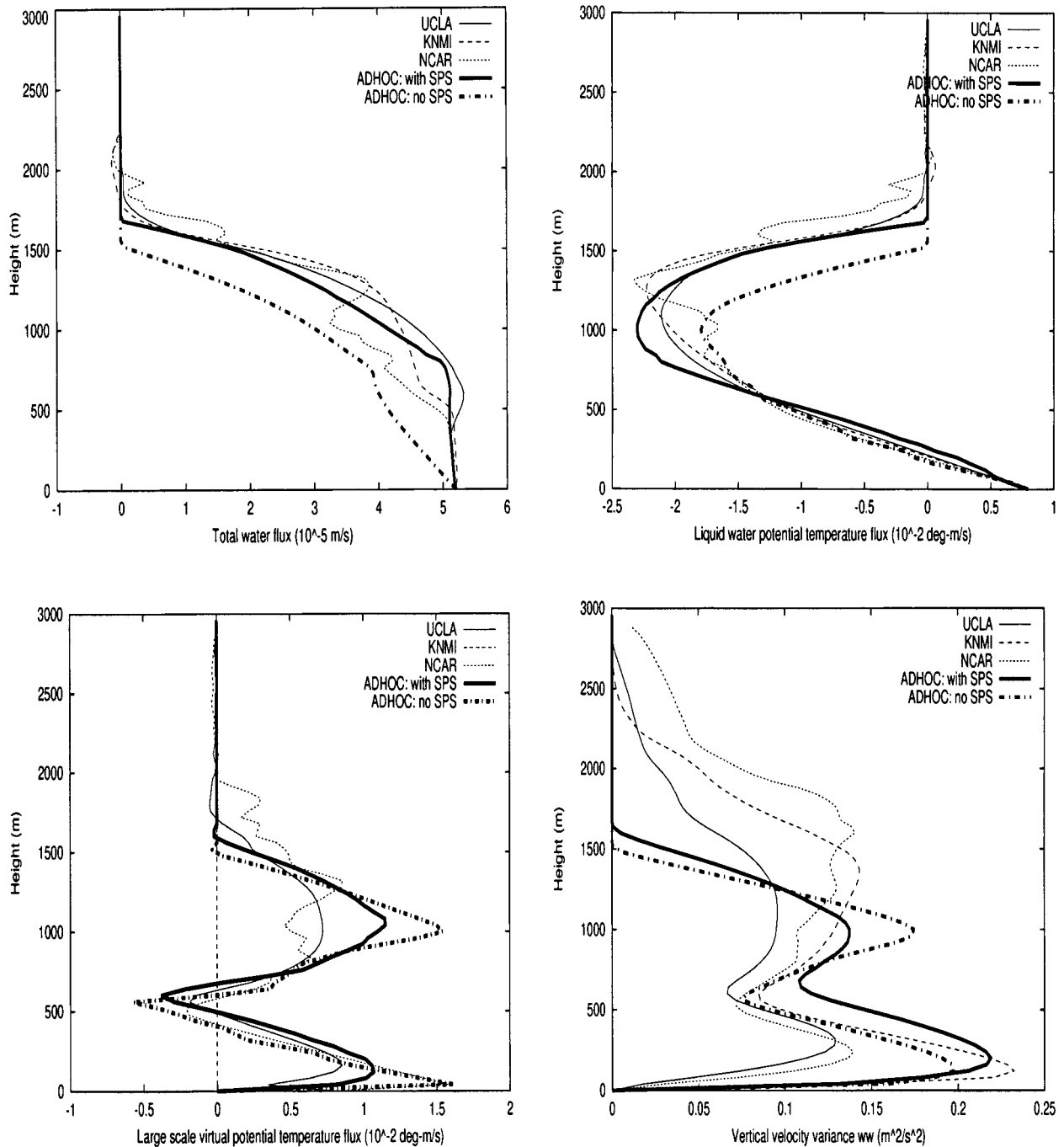


FIG. 7. Comparison of the ADHOC-simulated total water flux, liquid water, and virtual potential temperature fluxes, and the vertical velocity variance (for runs done with and without the inclusion of SPS motions) to those simulated by LES.

wind cumulus during BOMEX. The results show that the ADHOC approach is physically well suited for such a regime. We showed that the inclusion of SPS effects in this simulation was critical in order to capture the mean state and the turbulent structure of the cloud, as well as the proper mixing of turbulence near the surface. In LR3, we will show additional results from simulations of a wide variety of clear and cloudy regimes.

Acknowledgments. This research was funded by the National Aeronautics and Space Administration under Grant NAG1-1701 and Contract 960700 through the Jet Propulsion Laboratory, and by the National Science Foundation under Grant OPP9504246, all to Colorado State University. Computing support was obtained from the Scientific Computing Division of the National Center for Atmospheric Research. We would like to thank

Akio Arakawa and two anonymous reviewers for their helpful suggestions.

APPENDIX

A Toy Version of ADHOC

In order to explore the parameterizations for E and D discussed in section 2, a “toy model” was developed. In this model, we simplified the ADHOC equations as much as possible so that the flow could be more easily analyzed. We used this toy model to study the Willis–Deardorff laboratory convection experiment (Willis and Deardorff 1974, hereafter WD74), a relatively simple turbulent regime. The ADHOC equations were simplified by using known similarity relationships for free convection. The toy model uses the following simplifications.

- 1) The temperature is well mixed from the surface to the PBL top. This means that the temperature is constant and that heat flux is linear. We prescribe the surface heat flux based on the convection tank experiment (WD74), so the entire profile of $w'T'$ is known.
- 2) All higher moments are approximately in steady state.
- 3) There is no SPS motion.
- 4) The PBL-top height is preset.
- 5) The surface turbulent heat flux is preset (note that this, along with assumption 4, means that the PBL-top entrainment rate is also preset).
- 6) At any height, the turbulent length scale L_{dn} is the distance to the surface, while L_{up} is the distance to the PBL top.

In order to implement this model, we do the following.

- 1) Initialize $\overline{w'w'}$ using the known similarity relationship for free convection (Stull 1988).
- 2) Guess a profile of σ .
- 3) Vertically integrate the steady-state versions of the ADHOC continuity equation [Eq. (16)] to obtain M_c .
- 4) Solve for σ as a function of height using the ADHOC relationship,

$$\sigma(1 - \sigma) = \frac{M_c^2}{m^2 \overline{w'w'}}.$$

- 5) Iterate by returning to step 3 until σ has changed by less than 1%.

By following these steps, we essentially determine profiles of σ and M_c that are consistent with the similarity relationships for $\overline{w'w'}$ (note that this means we also know the profile of $w_{up} - w_{dn}$). The next step of the toy model determines E , D , and the pressure term Π . The three steady-state equations used by ADHOC for σ , $\overline{w'w'}$, and $\overline{w'T'}$ [see Eqs. (47)–(49) in LR1] are, respectively,

$$E - D - \frac{\partial}{\partial z}[m\sigma(1 - \sigma)(w_{up} - w_{dn})] = 0, \quad (A1)$$

$$\begin{aligned} & -(w_{up} - w_{dn})^2(E + D) \\ & - \frac{\partial}{\partial z}[m\sigma(1 - \sigma)(1 - 2\sigma)(w_{up} - w_{dn})^3] \\ & + 2g\alpha(\overline{mw'T'}) \\ & + 2m\sigma(1 - \sigma)(w_{up} - w_{dn})(\Pi_{up} - \Pi_{dn}) \\ & = 0, \end{aligned} \quad (A2)$$

$$\begin{aligned} & - \frac{(E + D)}{m\sigma(1 - \sigma)}(\overline{mw'T'}) \\ & - \frac{\partial}{\partial z}[(1 - 2\sigma)(w_{up} - w_{dn})(\overline{mw'T'})] \\ & + \frac{g\alpha}{m\sigma(1 - \sigma)}\left(\frac{\overline{mw'T'}}{w_{up} - w_{dn}}\right)^2 + (\overline{mw'T'})\left(\frac{\Pi_{up} - \Pi_{dn}}{w_{up} - w_{dn}}\right) \\ & = 0. \end{aligned} \quad (A3)$$

We can solve the system of equations (A1)–(A3) because they contain only three unknowns, namely, E , D , and $\Pi_{up} - \Pi_{dn}$ (we know all other terms from the exercise discussed above). We now can solve for the lateral mixing constants, $C_{ww,E}$ and $C_{ww,D}$. Note that they will be functions of height. These two variables are plotted in Fig. 2.

REFERENCES

- André, J. C., G. DeMoor, P. Lacarrere, and R. Du Vachat, 1976: Turbulence approximation for inhomogeneous flows. Part II: The numerical simulation of a penetrative convection experiment. *J. Atmos. Sci.*, **33**, 482–491.
- , —, —, G. Therry, and R. Du Vachat, 1978: Modeling the 24-hour evolution of the mean and turbulent structures of the planetary boundary layer. *J. Atmos. Sci.*, **35**, 1861–1883.
- Arakawa, A., and W. H. Schubert, 1974: The interaction of a cumulus cloud ensemble with the large-scale environment, Part I. *J. Atmos. Sci.*, **31**, 674–701.
- Batchelor, G. K., 1954: Heat convection and buoyancy effects in fluids. *Quart. J. Roy. Meteor. Soc.*, **80**, 339–358.
- Bechtold, P., J. W. M. Cuijpers, P. Mascart, and P. Trouilhet, 1995: Modeling of trade wind cumuli with a low-order turbulence model: Toward a unified description of Cu and Sc clouds in meteorological models. *J. Atmos. Sci.*, **52**, 455–463.
- Beljaars, A. C. M., J. L. Walmsley, and P. A. Taylor, 1987: Modeling of turbulence over low hills and varying surface roughness. *Bound.-Layer Meteor.*, **41**, 203–215.
- Blackadar, A. K., 1962: The vertical distribution of wind and turbulent exchange in neutral atmospheres. *J. Geophys. Res.*, **67**, 3095–3102.
- Bougeault, P., 1981: Modeling the trade wind cumulus boundary layer. Part II: High-order one-dimensional model. *J. Atmos. Sci.*, **38**, 2414–2428.
- , and J. C. André, 1986: On the stability of the third-order turbulence closure for the modeling of the stratocumulus-topped boundary layer. *J. Atmos. Sci.*, **43**, 1574–1581.
- Browning, K. A., 1994: Survey of perceived priority issues in the parameterizations of cloud-related processes. *Quart. J. Roy. Meteor. Soc.*, **120**, 483–487.

- Bretherton, C. S., and P. K. Smolarkiewicz, 1989: Gravity waves, compensating subsidence, and detrainment around cumulus clouds. *J. Atmos. Sci.*, **46**, 740–759.
- Businger, J. A., and S. P. Oncley, 1990: Flux measurements with conditional sampling. *J. Atmos. Oceanic Technol.*, **7**, 349–352.
- Canuto, V. M., 1992: Turbulent convection with overshooting: Reynolds stress approach. *Astrophys. J.*, **392**, 218–232.
- , F. Minotti, C. Ronchi, R. M. Ypma, and O. Zeman, 1994: Second-order closure PBL model with new third-order moments: Comparison with LES data. *J. Atmos. Sci.*, **51**, 1605–1618.
- Cuijpers, J. W. M., and P. G. Duynkerke, 1993: Large eddy simulation of trade wind cumulus clouds. *J. Atmos. Sci.*, **50**, 3894–3908.
- Deardorff, J. W., 1972: Numerical investigation of neutral and unstable planetary boundary layers. *J. Atmos. Sci.*, **29**, 91–115.
- , 1980: Stratocumulus-capped mixed layers derived from a three-dimensional model. *Bound.-Layer Meteorol.*, **18**, 495–527.
- de Laat, A. T. J., and P. G. Duynkerke, 1998: Analysis of ASTEX-stratocumulus observational data using mass-flux approach. *Bound.-Layer Meteorol.*, **86**, 63–87.
- de Roode, S. R., P. G. Duynkerke, and A. P. Siebesma, 2000: Analogies between mass-flux and Reynolds-averaged equations. *J. Atmos. Sci.*, **57**, 1585–1598.
- Detering, H. W., and D. Etling, 1985: Application of the E - ϵ turbulence model to the atmospheric boundary layer. *Bound.-Layer Meteorol.*, **33**, 113–133.
- Emanuel, K., 1991: A scheme for representing cumulus convection in large-scale models. *J. Atmos. Sci.*, **48**, 2313–2335.
- Esbensen, S., 1978: Bulk thermodynamic effects and properties of small tropical cumuli. *J. Atmos. Sci.*, **35**, 826–837.
- Gregory, D., and P. R. Rowntree, 1990: A mass-flux convection scheme with representation of cloud ensemble characteristics and stability-dependent closure. *Mon. Wea. Rev.*, **118**, 1483–1506.
- Heymsfield, A. J., P. N. Johnson, and J. E. Dye, 1978: Observations of moist adiabatic ascent in northeast Colorado cumulus congestus clouds. *J. Atmos. Sci.*, **35**, 1689–1703.
- Kain, J. S., and J. M. Fritsch, 1990: A one-dimensional entraining/detraining plume model and its application in convective parameterization. *J. Atmos. Sci.*, **47**, 2784–2802.
- Kolmogorov, A. N., 1942: Equations of turbulent motion of an incompressible fluid. *Izv. AN SSSR, Ser. fiz.*, **6**, 56–58.
- Langland, R. H., and C.-S. Liou, 1996: Implementation of an E - ϵ parameterization of vertical subgrid-scale mixing in a regional model. *Mon. Wea. Rev.*, **124**, 905–918.
- Lappen, C.-L., 1999: The unification of mass flux and higher-order closure in the simulation of boundary layer turbulence. Ph.D. thesis, Colorado State University, 330 pp.
- , and D. A. Randall, 2001a: Toward a unified parameterization of the boundary layer and moist convection. Part I: A new type of mass flux model. *J. Atmos. Sci.*, **58**, 2021–2036.
- , and —, 2001b: Toward a unified parameterization of the boundary layer and moist convection. Part III: Simulations of clear and cloudy convection. *J. Atmos. Sci.*, **58**, 2052–2072.
- Lin, C., and A. Arakawa, 1997: The macroscopic entrainment processes of simulated cumulus ensemble. Part II: Testing the entraining plume model. *J. Atmos. Sci.*, **54**, 1044–1053.
- Moeng, C.-H., 1984: A large-eddy-simulation for the study of planetary boundary-layer turbulence. *J. Atmos. Sci.*, **41**, 2052–2062.
- Morton, B. R., 1957: Buoyant plumes in a moist atmosphere. *J. Fluid Mech.*, **2**, 127–144.
- Petersen, A. C., C. Beets, H. van Dop, and P. G. Duynkerke, 1999: Mass-flux characteristics of reactive scalars in the convective boundary layer. *J. Atmos. Sci.*, **56**, 37–56.
- Randall, D. A., 1987: Turbulent fluxes of liquid water and buoyancy in partly cloudy layers. *J. Atmos. Sci.*, **44**, 850–858.
- , and G. J. Huffman, 1982: Entrainment and detrainment in a simple cumulus cloud model. *J. Atmos. Sci.*, **39**, 2793–2806.
- Raymond, D. J., 1979: A two-scale model of moist, non-precipitating convection. *J. Atmos. Sci.*, **36**, 816–831.
- , and M. Wilkening, 1982: Flow and mixing in New Mexico mountain cumuli. *J. Atmos. Sci.*, **39**, 2211–2228.
- , and A. M. Blyth, 1986: A stochastic mixing model for non-precipitating cumulus convection. *J. Atmos. Sci.*, **43**, 2708–2718.
- Schumann, U., and C.-H. Moeng, 1991: Plume fluxes in clear and cloudy convective boundary layers. *J. Atmos. Sci.*, **48**, 1746–1757.
- Scorer, R. S., 1957: Experiments on convective isolated masses of buoyant fluid. *J. Fluid Mech.*, **2**, 583–594.
- Siebesma, A. P., and J. W. M. Cuijpers, 1995: Evaluation of parametric assumptions for shallow cumulus convection. *J. Atmos. Sci.*, **52**, 650–666.
- , and A. A. M. Holtslag, 1996: Model impacts of entrainment and detrainment rates in shallow cumulus convection. *J. Atmos. Sci.*, **53**, 2354–2364.
- Simpson, J., 1971: On cumulus entrainment and one-dimensional models. *J. Atmos. Sci.*, **28**, 449–455.
- , and V. Wiggert, 1969: Models of precipitating cumulus towers. *Mon. Wea. Rev.*, **97**, 471–489.
- , R. H. Simpson, D. A. Andrews, and M. A. Eaton, 1965: Experimental cumulus dynamics. *Rev. Geophys.*, **3**, 387–431.
- Squires, P., 1958: Penetrative downdraughts in cumuli. *Tellus*, **10**, 381–389.
- , and J. S. Turner, 1962: An entraining jet model for cumulonimbus updraughts. *Tellus*, **4**, 422–434.
- Stevens, B., R. L. Walko, W. R. Cotton, and G. Feingold, 1996: Elements of the microphysical structure of numerically simulated nonprecipitating stratocumulus. *J. Atmos. Sci.*, **53**, 980–1007.
- Stommel, H., 1947: Entrainment of air into a cumulus cloud. *J. Meteorol.*, **4**, 91–94.
- Stull, R. B., 1988: *An Introduction to Boundary Layer Meteorology*. Kluwer Academic, 666 pp.
- Taylor, G. R., and M. B. Baker, 1991: Entrainment and detrainment in cumulus clouds. *J. Atmos. Sci.*, **48**, 112–121.
- Telford, J. W., 1975: Turbulence, entrainment, and mixing in cloud dynamics. *Pure Appl. Geophys.*, **113**, 1067–1084.
- Tiedtke, M., 1989: A comprehensive mass-flux scheme for cumulus parameterization in large-scale models. *Mon. Wea. Rev.*, **117**, 1779–1800.
- Turner, J. S., 1973: *Boundary Effects in Fluids*. Cambridge University Press, 337 pp.
- Wang, S., and B. Albrecht, 1986: Stratocumulus model with an internal circulation. *J. Atmos. Sci.*, **43**, 2374–2391.
- , and B. Stevens, 2000: Top-hat representation of turbulence statistics in cloud-topped boundary layers: A large eddy simulation study. *J. Atmos. Sci.*, **57**, 423–441.
- Warner, J., 1970: On steady-state one-dimensional models of cumulus convection. *J. Atmos. Sci.*, **27**, 1035–1040.
- Willis, G. E., and J. W. Deardorff, 1974: Laboratory model of the unstable planetary boundary layer. *J. Atmos. Sci.*, **31**, 1297–1307.
- Wyngaard, J. C., and C.-H. Moeng, 1992: Parameterizing turbulent diffusion through the joint probability density. *Bound.-Layer Meteorol.*, **60**, 1–13.
- Yamada, T., and G. L. Mellor, 1979: Numerical simulation of BOMEX data using a turbulence closure model coupled with ensemble cloud relations. *Quart. J. Roy. Meteor. Soc.*, **105**, 915–944.
- Young, G. S., 1988: Turbulence structure of the convective boundary layer. Part I: Variability of normalized turbulence statistics. *J. Atmos. Sci.*, **45**, 719–726.